◆ Human Brain Mapping 38:938–956 (2017) ◆

Structural and Functional Connectivity of the Precuneus and Thalamus to the Default Mode Network

Samantha I. Cunningham,[1]* Dardo Tomasi,[1] and Nora D. Volkow[1,2]

[1]*National Institutes of Health, NIAAA, Bethesda, Maryland*
[2]*National Institute of Health, NIDA, Bethesda, Maryland*

Abstract: Neuroimaging studies have identified functional interactions between the thalamus, precuneus, and default mode network (DMN) in studies of consciousness. However, less is known about the structural connectivity of the precuneus and thalamus to regions within the DMN. We used diffusion tensor imaging (DTI) to parcellate the precuneus and thalamus based on their probabilistic white matter connectivity to each other and DMN regions of interest (ROIs) in 37 healthy subjects from the Human Connectome Database. We further assessed resting-state functional connectivity (RSFC) among the precuneus, thalamus, and DMN ROIs. The precuneus was found to have the greatest structural connectivity with the thalamus, where connection fractional anisotropy (FA) increased with age. The precuneus also showed significant structural connectivity to the hippocampus and middle pre-frontal cortex, but minimal connectivity to the angular gyrus and midcingulate cortex. In contrast, the precuneus exhibited significant RSFC with the thalamus and the strongest RSFC with the AG. Significant symmetrical structural connectivity was found between the thalamus and hippocampus, mPFC, sFG, and precuneus that followed known thalamocortical pathways, while thalamic RSFC was strongest with the precuneus and hippocampus. Overall, these findings reveal high levels of structural and functional connectivity linking the thalamus, precuneus, and DMN. Differences between structural and functional connectivity (such as between the precuneus and AG) may be interpreted to reflect dynamic shifts in RSFC for cortical hub-regions involved with consciousness, but could also reflect the limitations of DTI to detect superficial white matter tracts that connect cortico-cortical regions. *Hum Brain Mapp 38:938–956, 2017.*

Key words: default mode network; precuneus; thalamus; diffusion tensor imaging; resting-state fMRI; Human Connectome Project

INTRODUCTION

The default mode network (DMN), which is involved with interoceptive awareness and mind wandering [Christoff et al., 2009; Jang et al., 2010; Taylor et al., 2013], has been proposed as a marker of an individual's degree of consciousness [Cauda et al., 2009; Crone et al., 2015; Hannawi et al., 2015; Soddu et al., 2012; Vanhaudenhuyse

Additional Supporting Information may be found in the online version of this article.

Contract grant sponsor: National Institutes of Health Intramural Research Program.

The authors declare no conflicts of interest.

*Correspondence to: Samantha I. Cunningham, Ph.D.; Postdoctoral Fellow in NIAAA's Laboratory of Neuroimaging, National Institutes of Health, MSC 1013, 10 Center Drive, Room B2L124, Bethesda, MD, 20892. E-mail: samicunn@gmail.com

Received for publication 17 August 2015; Revised 15 August 2016; Accepted 27 September 2016.

DOI: 10.1002/hbm.23429

Published online 14 October 2016 in Wiley Online Library (wileyonlinelibrary.com)

et al., 2010]. Connectivity of the DMN is reduced in proportion to a patient's level of impairment [Vanhaudenhuyse et al., 2010] and decreases in glucose metabolism have been observed in key regions of the DMN (including the precuneus) during states of impaired consciousness [Fridman et al., 2014; García-Panach et al., 2011; Laureys et al., 1999].

The thalamus, which is involved in alertness, has also been implicated in disorders of consciousness [White and Alkire, 2003]. Arthuis et al. [2009] described thalamocortical loops as pathways that coordinate conscious information processing from different regions of the brain. The thalamus—along with the precuneus [a central DMN hub: Gusnard and Raichle, 2001; Tomasi and Volkow, 2010; Utevsky et al., 2014; Zhang and Li, 2012]—has likewise been consistently associated with an individual's state of consciousness [Crone et al., 2013; Hannawi et al., 2015; Vanhaudenhuyse et al., 2010; Xie et al., 2011]. While the thalamus is not typically considered part of the DMN, resting-state studies have reported strong functional connectivity between the thalamus and the precuneus [Tomasi and Volkow, 2011; Zhang and Li, 2012]. These findings from fMRI serve to corroborate results from anatomical studies in non-human primates identifying bidirectional structural connections between precuneus and various thalamic nuclei [Cavanna and Trimble, 2006]. The relevance of the precuneus—along with other regions in the DMN and the thalamus—is highlighted by a study that showed altered structural connectivity (measured with DTI) among regions within the DMN, including a pathway connecting the precuneus and thalamus, in patients with impaired consciousness [Fernandez-Espejo et al., 2012].

Collectively, these findings suggest a strong relationship exists between consciousness and DMN connectivity to the precuneus and thalamus. However, while there have been studies of connectivity between the thalamus and precuneus to the rest of the brain [O'Muircheartaigh et al., 2015; Zhang and Li, 2012; Zhang et al., 2010], no systematic analysis to our knowledge has been completed that focuses on parcellation of the precuneus and thalamus based on their structural and functional connectivity to one another and regions of the DMN that could mediate the integrated brain activity required for consciousness. Here, we took advantage of open access, high-resolution diffusion (dMRI) and functional (fMRI) MRI data from the Human Connectome Database [Van Essen et al., 2013] to determine how the DMN is structurally connected to the thalamus and precuneus, and to identify functional resting-state connectivity between these regions. We hypothesized the existence of significant structural and functional connections between the thalamus and the precuneus and between these regions and other areas in the DMN. A detailed mapping of connectivity between the precuneus and thalamus and their connectivity with the DMN will provide a comprehensive baseline for future brain imaging studies, especially those involving consciousness.

MATERIALS AND METHODS

The methods described below are summarized as a step-by-step illustration in Figure 1.

Participants

Neuroimaging data from 37 healthy control subjects (17 males and 20 females, age range: 23–35 years) was obtained from the Human Connectome Project's (HCP) "WU-Minn HCP Data—900 Subjects" public dataset [Van Essen et al., 2013; http://www.humanconnectome.org/]. Specifically, our subjects were obtained from the "40 Unrelated Subjects" subset, which includes 38 pre-selected individuals from the larger database. One subject was excluded due to the presence of a normal midline calcification that would have interfered with region of interest (ROI)-based tractography analyses in that area. The scanning protocol was approved by Washington University in St. Louis's Human Research Protection Office (HRPO), IRB# 201204036. No experimental activity involving the human subjects took place at the authors' institutions. The participants included in this study provided written informed consent and were scanned according to procedures approved by the IRB at Washington University [Uğurbil et al., 2013].

Image Acquisition

Each subject underwent T1-weighted structural scans (TR/TE/T1/flip angle = 2.40 s/2.14 ms/1,000 ms/8°), spin-echo planar imaging (EPI) scans, diffusion-weighted scans (TR/TE/flip angle = 5.52 s/89.5 ms/78°, 1.25 mm isotropic voxels; multiband factor = 3), and resting-state gradient-echo EPI scans (TR/TE/flip angle = 720 ms/33.1 ms/52°, 1,200 time points; multiband factor = 8) in a Siemens 3T Connectome Skyra with a 32 channel coil. Diffusion-weighted data was acquired through six runs representing three different shells of $b = 1{,}000$, 2,000, and 3,000 s/mm^2 (including 90 diffusion weighting directions and 6 $b = 0$ acquisitions interspersed throughout each run), while functional connectivity analyses were performed on resting-state data acquired using a left-to-right phase encoding direction during the first of two scanning sessions.

All structural data had already been processed according to the HCP's minimal preprocessing pipeline, which included: spatial artifact/distortion removal, surface generation, cross-modal registration, and registration to MNI152 standard space [Glasser et al., 2013]. In addition, resting-state and diffusion data underwent further subsequent processing as described in Woolrich et al. [2001] and Andersson et al. [2003], respectively. For the resting-state dataset, this included: removal of spatial distortions, realignment of volumes to compensate for subjects' motion, and normalization of the 4D image to a global mean. For the diffusion dataset, this included: intensity normalization across runs, EPI distortion correction, eddy current and motion correction, and gradient nonlinearity correction.

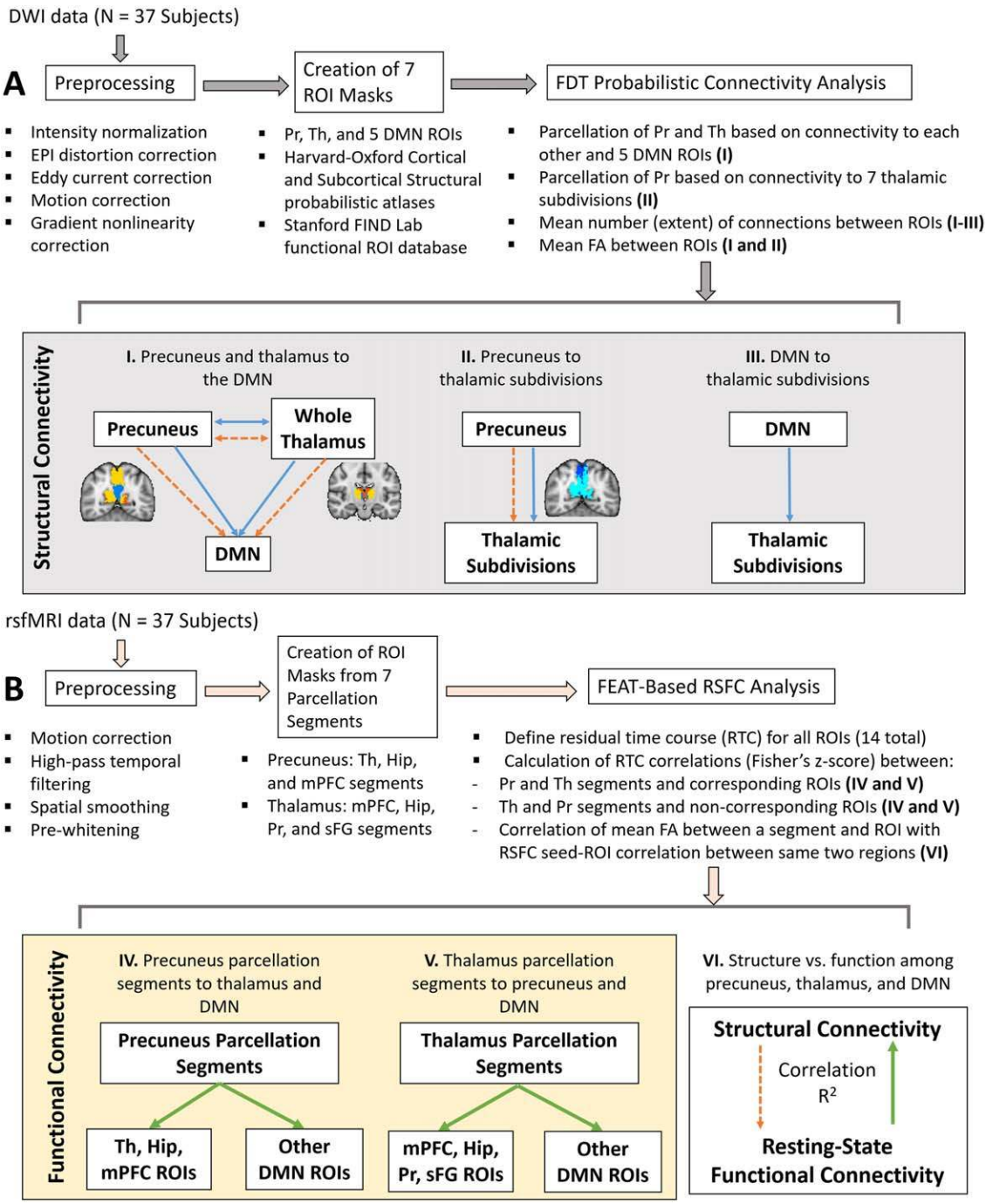

Figure 1.

Summary of structural and functional connectivity analysis methods. **A.** DWI-based probabilistic tractography analysis. **B.** Resting-state functional connectivity analysis. The mPFC segment of the precuneus and mPFC ROI are an example of a segment and its corresponding ROI, while the mPFC segment of the precuneus and AG ROI is an example of a segment and one of its non-corresponding ROIs. Blue solid lines = calculation of extent of white matter connections; orange dashed lines = calculation of mean FA between two regions; green solid lines = calculation of RSFC between a parcellation segment and ROI. [Color figure can be viewed at wileyonlinelibrary.com]

TABLE I. Illustration of the precuneus and thalamus target ROIs, as well as 5 key ROIs within the DMN [as described in Shirer et al., 2012]. [Color figure can be viewed at wileyonlinelibrary.com]

Full ROI Name	ROI ID	Illustration of ROI in MNI152 2 mm space
Precuneus	Pr	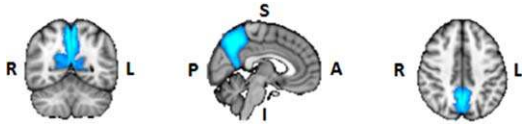
Thalamus	Th	
Angular Gyrus	AG	
Hippocampus	Hip	
Medial Prefrontal Cortex	mPFC	
Midcingulate Cortex	MCC	
Superior Frontal Gyrus	sFG	

ROI masks were obtained from FSL's Harvard-Oxford Cortical and Subcortical Structural probabilistic atlases [Desikan et al., 2006] and the Stanford FIND Lab functional ROI database [http://findlab.stanford.edu/functional_ROIs.html, Shirer et al., 2012]. ROI masks obtained from the probabilistic atlases (i.e. the Pr, Th, AG, Hip, and sFG) were thresholded in FSL at 50% signal intensity. All ROIs are superimposed on a standard MNI152 T1 2 mm resolution template brain for visualization purposes.

Selection of Regions of Interest

ROI masks for the diffusion and resting-state analyses were obtained from FSL's Harvard–Oxford Cortical and Subcortical Structural probabilistic atlases [Desikan et al., 2006], as well as the Stanford FIND Lab functional ROI database [http://findlab.stanford.edu/functional_ROIs.html, Shirer et al., 2012]; the use of probabilistic atlases in MNI152 provided us the flexibility of choosing an area within each mask that was highly represented among the population used to create the atlas. In addition to the precuneus and thalamus, five ROIs were selected from the DMN as described by Shirer et al. [2012], including: the angular gyrus (AG), hippocampus (Hip), midcingulate cortex (MCC), medial prefrontal cortex (mPFC), and superior frontal gyrus (sFG) (Table I). When assessing connectivity between the precuneus and regions within the thalamus, ROI masks were obtained from FSL's Oxford Thalamic Connectivity Probability Atlas and included seven subdivisions representing thalamic structural connections to the occipital lobe, posterior parietal lobe, prefrontal cortex, premotor cortex, primary motor cortex, sensory cortices, and temporal lobe [Behrens et al., 2003, Fig. 4B]. ROI masks obtained from the Cortical Structural, Subcortical Structural, and Thalamic Connectivity Probability Atlases (i.e., the AG, Hip, precuneus, sFG, thalamus, and seven thalamic subdivisions) were thresholded in FSL at 50% signal intensity. All ROIs were superimposed on a standard MNI152 T1 2 mm resolution template brain for visualization purposes (Table I and Figs. 1–8).

Diffusion-Weighted Data Analyses

Diffusion-weighted data was processed using FSL's diffusion toolbox [FDT, Behrens et al., 2003] and included:

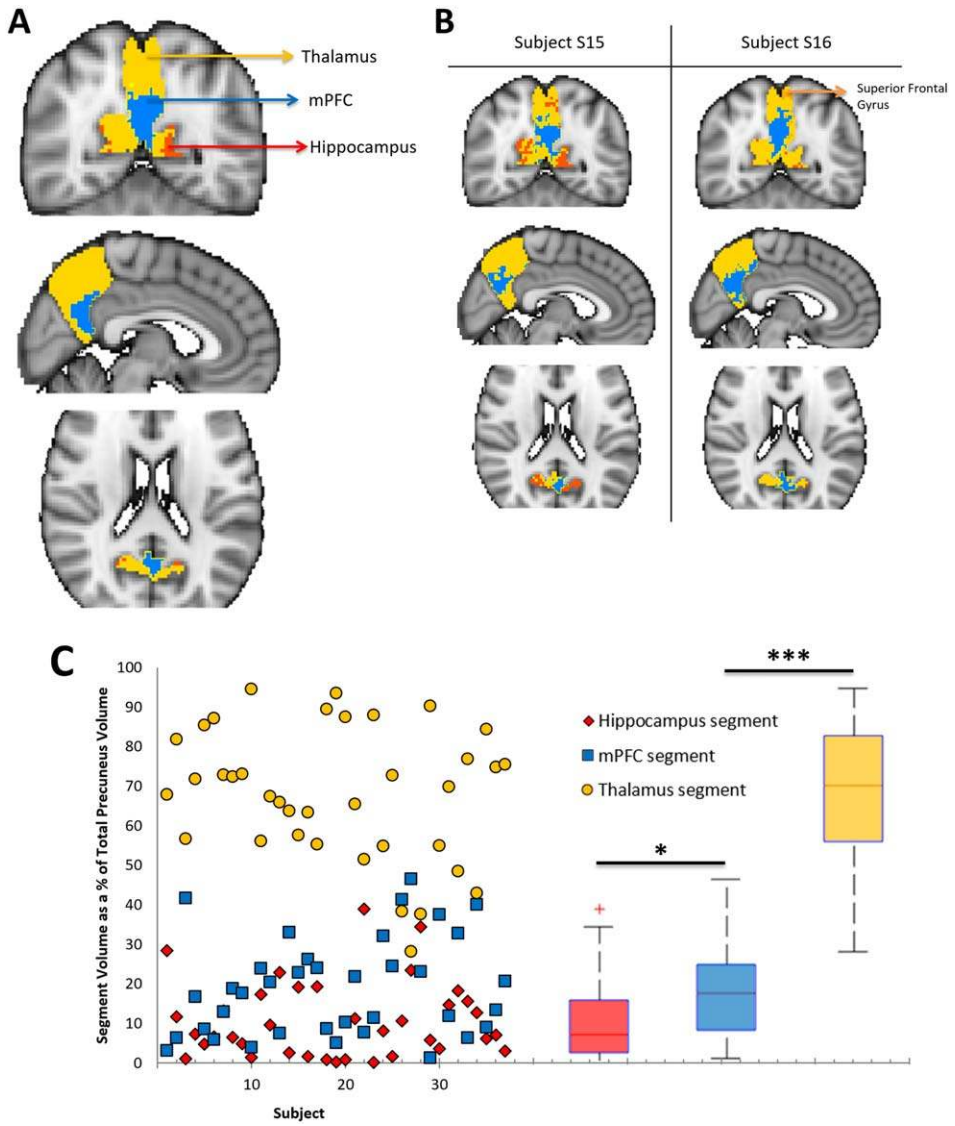

Figure 2.

Parcellation map of precuneus structural connectivity to the DMN, combined across 37 subjects. Across all subjects, each voxel of the precuneus was assigned to 1 of 6 target DMN ROIs (including the thalamus) based on the number of white matter connections to that region. **A.** Three of the 6 ROIs are represented on the combined precuneus map, which has been overlaid on a standard MNI152 2 mm isotropic template (yellow = thalamus, blue = mPFC, red = hippocampus). **B.** Parcellation maps from two representative subjects. **C.** Variability of segment volumes across subjects. Individual data points for each subject and segment are shown on the left. For each precuneus segment, boxplots on the right illustrate the distribution of volume values across subjects. The red line indicates the mean within each group, the edges of the boxes indicate the 25th and 75th percentiles, and the whiskers illustrate the most extreme data points. $^{*}P < 0.05$, $^{**}P < 0.001$, $^{***}P < 0.0001$. [Color figure can be viewed at wileyonlinelibrary.com]

fitting diffusion tensors to the corrected data, local modeling of diffusion parameters by fitting a probabilistic model to the corrected data, and probabilistic tractography based on this model. The resulting diffusion tensor images were then registered to MNI152 standard space with 2 × 2 × 2 mm isotropic resolution.

Structural connectivity of the precuneus and thalamus to the DMN

In order to determine how the DMN is structurally represented in the precuneus and thalamus, dMRI data was used to segment the precuneus and thalamus based on

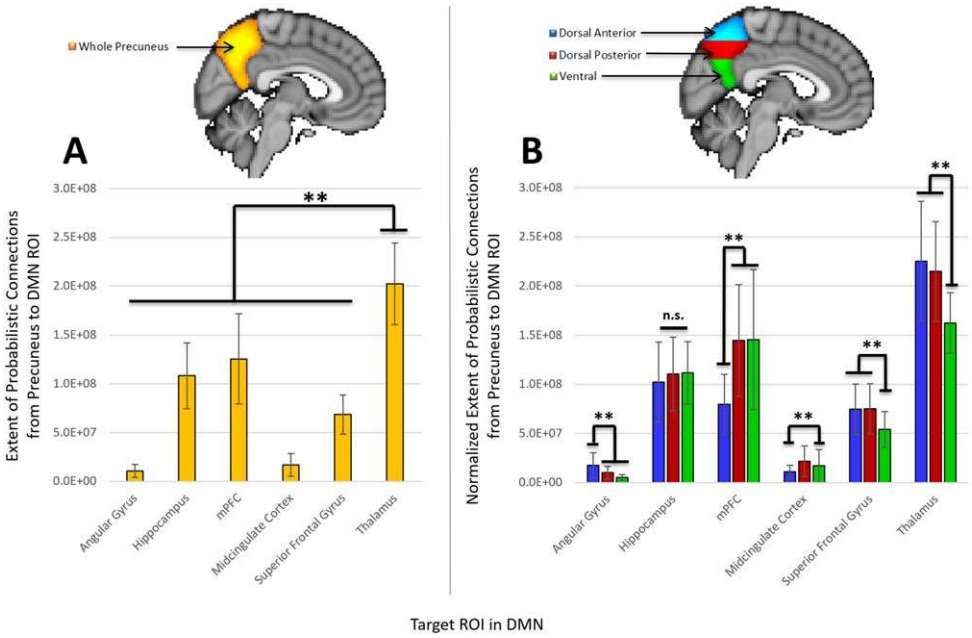

Figure 3.

Extent of structural connections between the precuneus and 6 target ROIs in the DMN. **A**: Extent of connections from the whole precuneus to each DMN ROI (including the thalamus). **B**: Extent of connections from the dorsal anterior (blue), dorsal posterior (red), and ventral (green) regions of the precuneus to each DMN ROI. The extent of connections from a precuneus subdivision has been normalized according to the volume of that particular subdivision. All values have been weighted based on the distance between ROIs and are therefore greater than the number of connections without distance correction. $^{*}P < 0.05$, $^{**}P < 0.01$, $^{***}P < 0.001$, n.s. = not significant. [Color figure can be viewed at wileyonlinelibrary.com]

their probabilistic connectivity to the five other DMN ROIs and each other. Parcellation maps for each subject were created using probabilistic tractography in FSL to determine the number of streamlines (out of 5,000) from each voxel of (1) the precuneus and (2) the thalamus that had a 50% chance or greater of reaching each target DMN ROI. Each voxel of the precuneus or thalamus was then assigned to the DMN ROI that received the highest number of streamlines (i.e., connections) from that voxel. The combined voxels representing an ROI defined a parcellation "segment" on the precuneus or thalamus. We determined the volume of each segment and used descriptive statistics to describe variability (in terms of mean and standard deviation) in segment volumes across subjects.

We further determined the degree of structural connectivity between the DMN and either precuneus or thalamus. The extent of structural connectivity was first defined as the mean number of connections reaching a target DMN ROI from either the precuneus or thalamus. In addition, the precuneus was divided into ventral, posterior dorsal, and anterior dorsal regions [as described in Zhang and Li, 2012] to identify differences in structural connectivity between each DMN ROI and these three subdivisions, where the mean number of connections was normalized according to the volume of each precuneus subdivision. In order to correct for the fact that structural connectivity decreases with distance from each ROI seed mask, the connectivity distribution between two ROIs was corrected for the distance between them using a distance weighting option in FSL's tractography processing scheme, as described below:

$$\text{Connectivity distribution for } \textit{voxel } A = \frac{l}{N},$$

where l refers to the length of pathways that cross *voxel A* (i.e., the number of voxels a streamline passes between two ROI seed masks), and N refers to the number of streamlines that cross *voxel A*. Instead of defining the connectivity distribution as the number of streamlines between two regions, the distance correction option also defines the path distribution in terms of the length of pathways. This ensured the parcellations were driven by remote connectivity as opposed to local connectivity by up-weighting streamlines farther from the seed ROI. All mean number of connections reported in the text include this distance correction and are reported as the "extent" of structural connectivity, where distance correction results in values that are greater than the true number of connections between two ROIs. Connections between the DMN and either precuneus or thalamus were further defined in

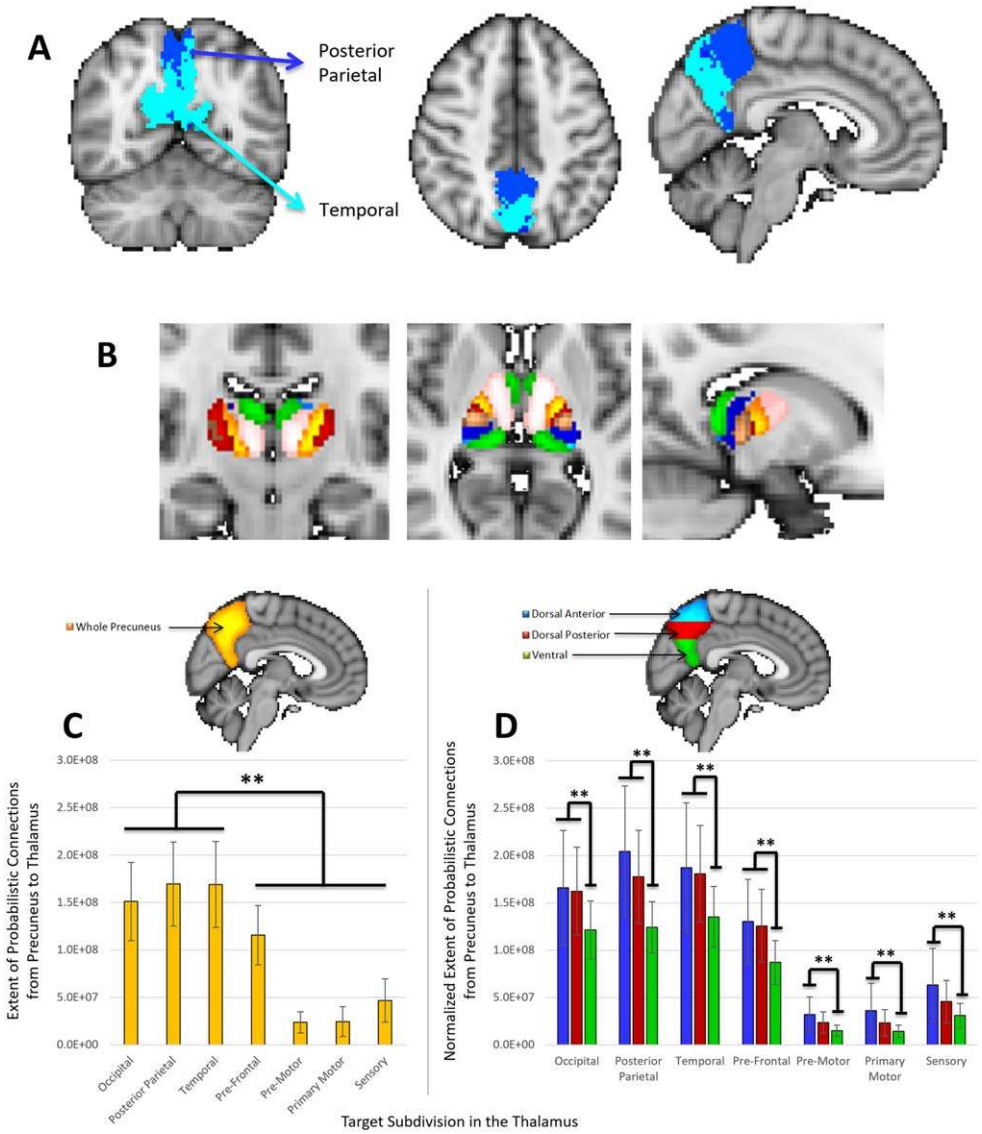

Figure 4.

Extent of structural connections between the precuneus and 7 thalamic subdivisions. **A**: Parcellation map of connectivity between the precuneus and thalamic subdivisions, combined across 37 subjects. The posterior parietal (dark blue) and temporal (light blue) divisions of the thalamus are the mostly strongly represented regions in the precuneus (NOTE: the posterior parietal and occipital subdivision ROIs overlapped considerably). **B.** Illustration of thalamic subdivisions (pink = prefrontal, yellow = premotor, red = primary motor, dark blue = posterior parietal, light blue = occipital, green = temporal, brown = sensory). ROIs were obtained from FSL's Oxford Thalamic Connectivity Probability Atlas [Behrens et al., 2003], thresholded in FSL at 50% signal intensity, and superimposed on a standard MNI152 T1 2 mm resolution template brain for visualization purposes. **C**: Extent of connections from the whole precuneus to each thalamic subdivision. **D**: Extent of connections from the dorsal anterior (blue), dorsal posterior (red), and ventral (green) regions of the precuneus to each thalamic subdivision. The extent of connections from a precuneus subdivision has been normalized according to the volume of that particular subdivision. All values have been weighted based on the distance between ROIs and are therefore greater than the number of connections without distance correction. $^{*}P < 0.05$, $^{**}P < 0.01$, $^{***}P < 0.001$. [Color figure can be viewed at wileyonlinelibrary.com]

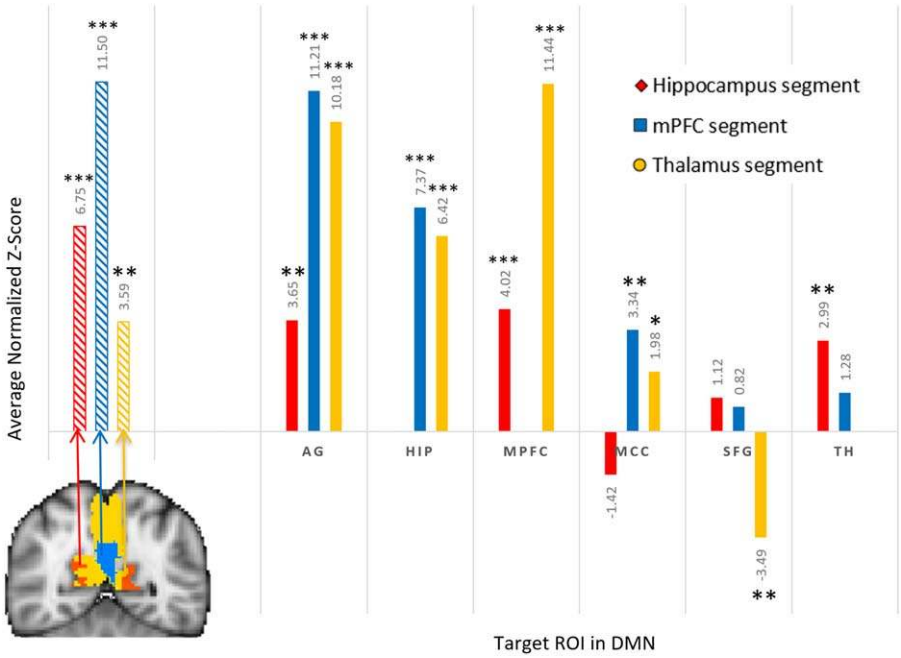

Figure 5.

Resting-state seed-ROI correlation between each of three precuneus structural segments and the thalamus and DMN ROIs. The resting-state seed-ROI correlation between two regions was defined as the Fisher's z-score averaged and normalized across subjects. The three stripped bars on the left of the graph illustrate the resting-state seed-ROI correlation between a precuneus segment and its corresponding DMN ROI, while solid bars on the right illustrate seed-ROI correlations between the three segments and their non-corresponding DMN ROIs. Exact average normalized z-scores are provided above each bar. $^{*}P < 0.05$, $^{**}P < 0.001$, $^{***}P < 0.0001$ indicate significance of the average normalized z-scores. [Color figure can be viewed at wileyonlinelibrary.com]

terms of the mean fractional anisotropy (FA) value along the distance-corrected tracts between two regions.

Differences in local functional connectivity density (*l*FCD) have been found between men and women among regions of the DMN, including the ventral precuneus and anterior thalamus [Tomasi and Volkow, 2012], while an age-related decrease in functional connectivity has also been observed in the DMN [Sambataro et al., 2010]. In an effort to determine if similar differences were observed for structural connectivity between DMN ROIs, a one-way multivariate analysis of variance (MANOVA) and correlation analyses were used to identify any effects of gender and age, respectively, on segment volumes and the extent of connections and FA values between two regions. In addition, mean FA values were evaluated as a function of extent of connectivity for each ROI pair. Significance thresholds were corrected for multiple comparisons ($\alpha = 0.05/6$ target ROIs $= 0.008$).

Structural connectivity between the precuneus and thalamic subdivisions

In order to determine how the precuneus is structurally connected to different regions within the thalamus, we similarly calculated the number of streamlines from each voxel of the precuneus that had a 50% chance or greater of reaching each of seven thalamic subdivisions [as defined according to the Oxford Thalamic Connectivity Probability Atlas: Behrens et al., 2003, Fig. 4B]. Each voxel of the precuneus was then assigned to the thalamic subdivision that received the highest number of connections from that voxel. The "extent" of structural connectivity was defined as the mean number of connections with a 50% chance or greater of reaching a thalamic subdivision from the precuneus. Similar to above, the precuneus was divided into ventral, posterior dorsal, and anterior dorsal regions to identify differences in structural connectivity between each thalamic subdivision and the three precuneus subdivisions, where the mean number of connections was normalized according to the volume of each precuneus subdivision and corrected for the distance between the precuneus and each thalamic subdivision. We then determined the mean FA value of connections between two regions. Significance thresholds were corrected for multiple comparisons ($\alpha = 0.05/7$ thalamic subdivision ROIs $= 0.007$).

Structural connectivity of thalamic subdivisions to the DMN

We further investigated whether structural connectivity between the thalamus and DMN follows thalamocortical

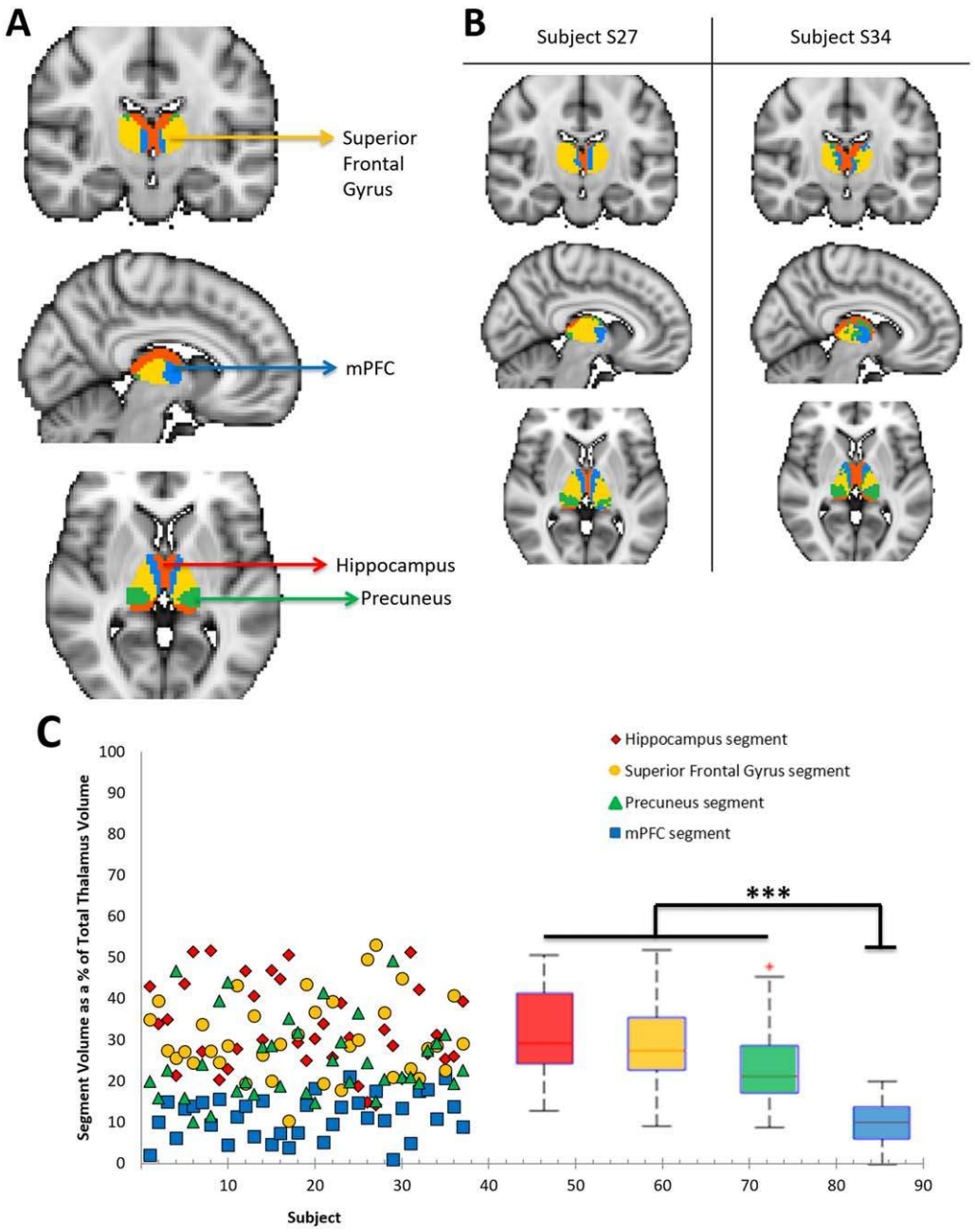

Figure 6.

Parcellation map of thalamic structural connectivity to the DMN, combined over 37 subjects. Across all subjects, each voxel of the thalamus was assigned to 1 of 6 target DMN ROIs based on the number of white matter connections to that region. **A.** Four of the 6 ROIs are represented on the combined thalamus map, which has been overlaid on a standard MNI152 2 mm isotropic template (yellow = sFG, blue = mPFC, red = hippocampus, green = precuneus). **B.** Two representative subjects are shown on the right. **C.** Variability of segment volumes across subjects. Individual data points for each subject and segment are shown on the left. For each thalamus segment, boxplots on the right illustrate the distribution of volume values across subjects. The red line indicates the mean within each group, the edges of the boxes indicate the 25th and 75th percentiles, and the whiskers illustrate the most extreme data points. $^{*}P < 0.05$, $^{**}P < 0.001$, $^{***}P < 0.0001$. [Color figure can be viewed at wileyonlinelibrary.com]

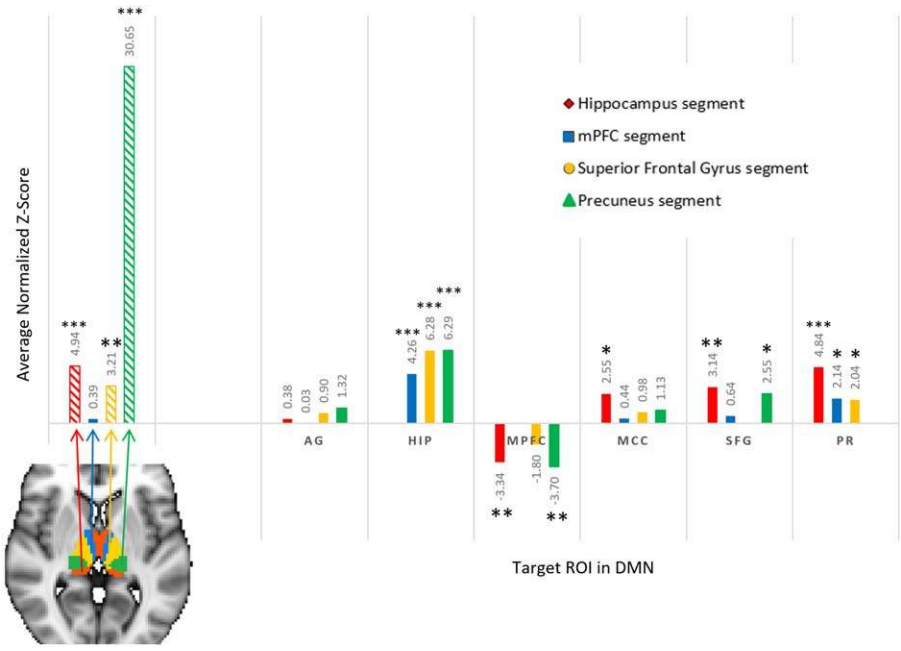

Figure 7.

Resting-state seed-ROI correlation between each of four thalamus segments and six DMN ROIs. The resting-state seed-ROI correlation between two regions was defined as the Fisher's z-score averaged and normalized across subjects. The four stripped bars on the left of the graph illustrate the resting-state seed-ROI correlation between a thalamus segment and its corresponding DMN ROI, while solid bars on the right illustrate seed-ROI correlations between the four segments and their non-corresponding DMN ROIs. Exact average normalized z-scores are provided above each bar. $^{*}P < 0.05$, $^{**}P < 0.001$, $^{***}P < 0.0001$ indicate significance of the average normalized z-scores. [Color figure can be viewed at wileyonlinelibrary.com]

pathways defined according to the Oxford Thalamic Connectivity Probability Atlas [Fig. 4B, Behrens et al., 2003]. This atlas describes the probabilistic connectivity between the thalamus and regions throughout the cortex that correspond well with previous anatomical animal studies. For example, correspondence between tractography findings in humans and the anatomical results in non-human primates were observed for connections between the following thalamic nuclei: the mediodorsal nucleus and the prefrontal cortex [Tanaka, 1976; Tobias, 1975], the ventral posterior nucleus and the somatosensory cortex [Jones and Powell, 1970], a combined ventral lateral and ventral anterior and the motor cortex [Jones et al., 1979], and between the combined lateral posterior nucleus and the pulvinar and the posterior parietal cortex [Jones, 1985]. To identify which thalamic subdivisions received the most structural connections from each DMN ROI, we calculated the mean number of connections from each DMN ROI to each subdivision of the thalamus. Using the results of our probabilistic tractography analysis from the thalamus as a whole to each DMN ROI (described above in "*Structural connectivity of the precuneus and thalamus to the DMN*"), each thalamus subdivision was used as a mask to isolate connections along the probabilistic pathway that terminated in voxels within that subdivision. A student's *t*-test (two-tailed, unequal variances) was then used to determine which thalamic subdivision(s) received a significantly greater number of connections from a particular DMN ROI when compared with other subdivisions (significance thresholds were corrected for multiple comparisons [$\alpha = 0.05/7$ thalamic subdivision ROIs $= 0.007$]). For example, if the mPFC ROI was found to have significantly greater structural connectivity to the frontal lobe subdivision of the thalamus, it could be concluded that connectivity between the mPFC and the thalamus follows a known thalamocortical pathway [as defined by Behrens et al., 2003] connecting the thalamus to the frontal regions of the cortex.

Resting-State Data Analyses

Resting-state data was processed using FSL's fMRI Expert Analysis Tool (FEAT) and included motion correction [using FSL's MCFLIRT tool, Jenkinson et al., 2002], high-pass temporal filtering (high-pass filter cutoff = 864 s), spatial smoothing (FWHM = 5 mm), and registration to MNI152 2 × 2 × 2 mm standard space. FILM pre-whitening was used to minimize the impact of temporal autocorrelation without affecting the functional connectivity results [Arbabshirani et al., 2014]. Low-pass filtering was not used

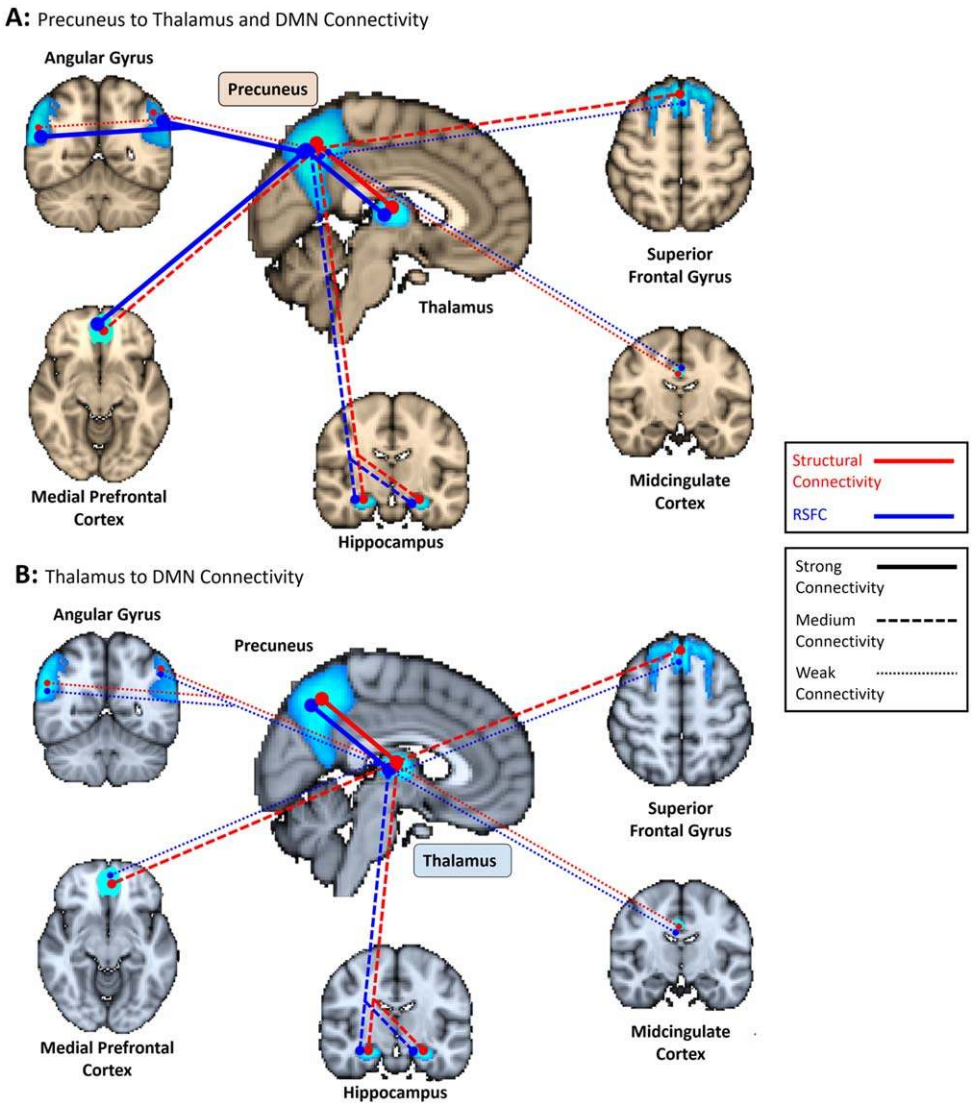

Figure 8.

Summary of structural (red lines) and functional (blue lines) connectivity among the precuneus, thalamus, and DMN. **A.** Connectivity from the precuneus to thalamus and 5 DMN ROIs. **B.** Connectivity from the thalamus to 6 DMN ROIs (including the precuneus). Differences in connectivity between the precuneus and thalamus for panel A versus B is a result of our analysis methods: for structure, the parcellation was completed by only including connections that started in one ROI and terminated in a 2nd ROI. This yielded different results when connections began in the precuneus versus the thalamus (since the precuneus ROI contains more voxels, more streamlines were sent to the thalamus than the smaller thalamus sent out to the precuneus, revealing more extensive connections). For function, RSFC was evaluated between the DMN ROIs and (1) structural segments of the thalamus and (2) structural segments of the precuneus. For example, the overall strength of functional connectivity from the thalamus to the precuneus was determined by averaging the z-scores from each thalamus segment to the precuneus. Since a segment of the thalamus (the "precuneus segment") had a much greater RSFC to the precuneus than any precuneus segments had to the thalamus, Pr-Th connectivity in Panel B is stronger than in Panel A. This means that from a parcellation point-of-view, the thalamus's structural segments were more functionally connected to the precuneus than the precuneus' segments were to the thalamus. Structure: strong connectivity $> 1.5 \times 10^8$ (bold lines), medium connectivity $= 5 \times 10^7$ to 1.5×10^8 (dashed lines), weak connectivity $< 5 \times 10^7$ normalized average probabilistic connections (dotted lines). Function: strong connectivity > 8 (bold lines), medium connectivity $= 5$ to 8 (dashed lines), weak connectivity < 5 average normalized z-score (dotted lines). [Color figure can be viewed at wileyonlinelibrary.com]

in order to avoid reducing signal strength and sensitivity [Della-Maggiore et al., 2002; Skudlarski et al., 1999].

Image data from the resting-state scans was used to assess functional connectivity between structure-based parcellation segments identified in the precuneus and thalamus and their corresponding DMN ROIs for each subject. These segments corresponded in the precuneus to the thalamus, hippocampus, and mPFC ROIs (Fig. 2), and in the thalamus to the mPFC, hippocampus, precuneus, and sFG ROIs (Fig. 6). For each segment—corresponding ROI pair (e.g., the mPFC segment of the precuneus and mPFC ROI), we defined the residual time course for each ROI as the BOLD response remaining after having removed activities attributable to white matter activity, non-neuronal responses in the ventricles, and time series of the remaining five non-corresponding DMN ROIs. These unwanted signals were extracted from the processed resting-state image data using FSL and removed via a partial correlation analysis using MATLAB's statistical processing toolbox (http://www.mathworks.com/products/statistics/), where the three activities described above served as the controlling variables. The resulting partial correlation, in terms of r, between the residual time courses of each segment and ROI in a pair (e.g., between the residual time course of the precuneus' mPFC segment and residual time course of the mPFC ROI) was taken to define the resting-state functional connectivity (RSFC) between the two regions. R-values for each subject were then converted to Fisher's z-scores using Fisher's transform and averaged across subjects for each segment—ROI pair. Average Fisher's z-scores were normalized using the standard error mean (SEM); P-values were assigned based on the average normalized z-score ($\alpha = 0.05$) for a segment—ROI pair. Descriptive statistics were used to describe variability of RSFC across subjects in terms of mean and standard deviation. One-way MANOVA and correlation analyses were further used to identify any effects of gender and age, respectively, on resting-state seed—ROI correlations for each segment—corresponding ROI pair. Significance thresholds were corrected for multiple comparisons (for precuneus segments: $\alpha = 0.05/3$ precuneus segments $= 0.017$; for thalamic segments: $\alpha = 0.05/4$ thalamic segments $= 0.013$).

Resting-state partial correlations were also calculated between each segment and their five non-corresponding ROIs. For example, separate partial correlations, in terms of r, were calculated between the mPFC segment of the precuneus and the (1) AG, (2) hippocampus, (3) MCC, (4) sFG, and (5) thalamus ROIs. Average normalized Fisher's z-scores for each pair were calculated across subjects and compared with the z-score between the same segment and its corresponding ROI using a student's t-test (two-tailed, unequal variances). This allowed us to identify the presence of resting-state specificity for each segment, where specificity was defined as a greater resting-state seed-ROI correlation (in terms of average normalized Fisher's z-score) between a segment and its corresponding ROI when compared with resting-state seed-ROI correlations between the same segment and its non-corresponding ROIs.

Finally, the relationship between structure and function within the DMN (including the precuneus) and with the thalamus was evaluated by correlating the mean FA value between a segment and ROI with the RSFC seed-ROI correlation between those same two regions.

RESULTS

Significant results discussed below and their effect sizes are summarized in Supporting Information Table S1 for clarity.

Structural connectivity of the precuneus to the thalamus and DMN

A parcellation map of precuneus structural connectivity revealed that the thalamus had the strongest representation in the precuneus, followed by the mPFC and hippocampus (Fig. 2A, B), whereas the other three DMN ROIs had minimal representation. While the volume of these segments in the precuneus varied across subjects, the thalamus segment ($68.11\% \pm 16.53\%$ of the total precuneus volume) was significantly larger (student's t-test [two-tailed, unequal variances], P's < 0.0001, Fig. 2C) than the mPFC ($18.94\% \pm 12.31\%$) and hippocampus segments ($10.72\% \pm 9.57\%$).

A one-way MANOVA (dependent variables: thalamus, hippocampus, and mPFC segment volumes; fixed factor: gender) and correlation analysis found no statistically significant effect of gender or age on the volume of these precuneus segments (P's > 0.50), respectively.

The extent of connectivity between the precuneus and DMN was further evaluated based on the number of connections that had a 50% chance or greater of existing between the precuneus and (1) each DMN ROI and (2) the thalamus (after correcting for the distance between ROIs, see *Methods Section "Diffusion-Weighted Data Analyses"*). In a similar manner to the parcellation map, results in 37 subjects revealed that the precuneus had significantly more extensive connections to the thalamus [$(20.2 \pm 4.2) \times 10^7$] than to any of the other 5 DMN ROIs (one-way ANOVA and Tukey post-hoc test, P's < 0.008), followed by the mPFC [$(12.5 \pm 4.6) \times 10^7$] and hippocampus [$(10.8 \pm 3.4) \times 10^7$, Fig. 3A], which both had significantly more extensive connections to the precuneus than the remaining three ROIs (P's < 0.008). Structural connections from the thalamus were further found to primarily target the anterior and posterior dorsal regions of the precuneus (one-way ANOVA and Tukey post-hoc test, P's < 0.008, Fig. 3B). Overall, a one-way ANOVA revealed that the anterior and posterior dorsal regions of the precuneus received significantly more extensive connections from the thalamus than any other DMN ROIs (P's < 0.008), while the ventral region received more extensive connections from the thalamus and mPFC (P's < 0.008).

A one-way MANOVA (dependent variables: number of connections OR FA values between the precuneus and AG, hippocampus, mPFC, MCC, sFG, and thalamus; fixed factor: gender) found no significant effect of gender on the extent or FA of connections between the precuneus and six target ROIs after correcting for multiple comparisons (P's > 0.03). However, a significant positive correlation was observed between age and mean FA values between the precuneus and thalamus across subjects ($r = 0.173$, $P = 0.005$), while a significant negative correlation between age and extent of connections was found between the same two regions ($r = -0.506$, $P = 0.001$). This suggests a decrease in the number and increase in the FA of structural connections between the thalamus and precuneus as age progresses from 23 to 35 years old.

Structural connectivity of the precuneus to thalamic subdivisions

Given the large structural representation of the thalamus in the precuneus, we sought to identify which regions of the thalamus had the most extensive structural connectivity to the precuneus. Target ROIs were based on thalamic subdivisions described in FSL's Oxford Thalamic Connectivity Probability Atlas [Behrens et al., 2003, Fig. 4B]. A one-way ANOVA and Tukey post-hoc test revealed that the precuneus received a significantly greater number of connections from the occipital, posterior parietal, and temporal subdivisions of the thalamus than any other subdivisions (P's < 0.007, Fig. 4C). In addition, thalamic subdivisions were primarily connected to the anterior and posterior dorsal regions of the precuneus (one-way ANOVA and Tukey post-hoc test, P's < 0.007, Fig. 4D), thus corroborating structural connectivity results described between the precuneus subdivisions and thalamus ROI (see *Results section "Structural connectivity of the precuneus to the thalamus and DMN"*). Despite a correlation being observed between age and mean FA values between the precuneus and whole thalamus ROI (see *Results section "Structural connectivity of the precuneus to the thalamus and DMN"*), no correlations between age and FA or number of connections between the precuneus and individual thalamic subdivisions were found (P's > 0.10).

Resting-state connectivity of the precuneus structural segments to the thalamus and DMN

In order to determine if strong structural connectivity underlies significant functional connectivity between the precuneus and thalamus and between the precuneus and DMN, we evaluated the RSFC seed-ROI correlation between each precuneus parcellation segment and its corresponding ROI (e.g., between the mPFC segment of the precuneus and mPFC ROI). Each precuneus segment was found to have a significant RSFC seed-ROI correlation with its corresponding ROI (11.50 > normalized average z-scores > 3.59, P's < 0.001, Fig. 5 left). While tractography revealed that the precuneus had a stronger structural connection with the thalamus than with DMN ROIs, RSFC revealed that the precuneus exhibited greater functional connectivity with DMN ROIs (i.e., the AG, mPFC and hippocampus) than with the thalamus. Even the precuneus' thalamus segment exhibited stronger RSFC with the AG than with the thalamus itself (student's t-test [two-tailed, unequal variances], $P < 0.001$).

No significant effect of gender (one-way MANOVA; dependent variables: resting-state seed-ROI correlations between precuneus segments [hippocampus, mPFC, thalamus] and corresponding ROIs [hippocampus, mPFC, thalamus]; fixed factor: gender) was found on RSFC between the precuneus segments and corresponding ROIs. However, a significant negative correlation was found between age and RSFC between the precuneus' thalamus segment and thalamus ($r = -0.418$, $P = 0.01$), where RSFC between the two regions decreased with age.

Each precuneus segment had variable RSFC to its non-corresponding ROIs. Across precuneus segments, the strongest RSFC seed-ROI correlations in addition to the AG were with the hippocampus and mPFC ROIs (11.44 > average normalized z-scores > 3.653, P's < 0.001, Fig. 5 right). The precuneus' thalamus segment exhibited a significant RSFC seed-ROI correlation to all other DMN ROIs (11.44 > average normalized z-scores > 1.98, P's < 0.05). However, RSFC in the hippocampus segment was not significantly correlated with activity in the MCC and sFG (P's > 0.10), while the mPFC segment exhibited non-significant correlations to the sFG and thalamus (P's > 0.10).

Structural connectivity of the thalamus to the DMN

Results revealed a highly symmetrical representation of the hippocampus, sFG, precuneus, and mPFC across both hemispheres of the thalamus (Fig. 6A, B). This coincided with the four DMN ROIs having a significantly more extensive connections to the thalamus [hippocampus average number of connections = $(10.3 \pm 2.1) \times 10^7$; sFG = $(10.3 \pm 2.4) \times 10^7$; precuneus = $(9.9 \pm 1.9) \times 10^7$; mPFC = $(7.8 \pm 1.4) \times 10^7$] than the MCC = $(4.2 \pm 3.9) \times 10^6$ and AG = $(3.2 \pm 1.3) \times 10^6$ (one-way ANOVA and Tukey post-hoc test, P's < 0.008). Within the thalamus, the hippocampus segment (33.06% ± 10.55% of total thalamus volume), sFG segment (30.34% ± 9.32%), and precuneus segment (25.20% ± 9.71%) all had a significantly greater volume than the mPFC segment (11.36% ± 5.15%, $P < 0.0001$, Fig. 6C).

A one-way MANOVA (dependent variables: hippocampus, mPFC, sFG, and precuneus segment volumes; fixed factor: gender) found no significant effect of gender on the volume of the thalamus segments (P's > 0.10). However, significant correlations were found between age and volume of the mPFC segment ($r = 0.496$, $P = 0.002$) and precuneus segment ($r = -0.404$, $P = 0.013$), where older subjects

exhibited a larger mPFC segment and smaller precuneus segment.

The AG, hippocampus, mPFC, sFG, and precuneus all had a similar extent of connections to both hemispheres of the thalamus (student's *t*-test [two-tailed, unequal variance], P's > 0.05), whereas the MCC was more strongly represented in the right thalamus ($P = 0.0001$). A significant negative correlation was found between the average extent of connections and mean FA value between the thalamus and combined DMN ROIs ($r = -0.218$, $P = 0.0011$), where DMN regions with more extensive connections to the thalamus exhibited lower FA values; this was similar to the finding that FA and extent of connections between the precuneus and thalamus varied inversely with age (*see Results section "Structural connectivity of the precuneus to the thalamus and DMN"*).

When compared with thalamic subdivisions defined in the Oxford Thalamic Connectivity Probability Atlas (Fig. 4B), the location of each DMN segment was consistent with previously identified cortical and thalamic endpoints of white matter connections between the thalamus and cortex [Behrens et al., 2003]: when compared with other thalamic subdivisions, thalamus voxels projecting to the mPFC and sFG were primarily contained in the thalamic subdivision that projects to the pre-frontal cortex (see *Methods section "Diffusion-Weighted Data Analyses,"* P's < 0.01); precuneus connectivity was mainly associated with the thalamic subdivision that projects to the posterior parietal lobe (P's < 0.01); and thalamus voxels projecting to the hippocampus were primarily located in a subdivision that projects to the temporal lobe (P's < 0.01).

Resting-state connectivity of the thalamus structural segments to the DMN

In the same manner as the precuneus, the RSFC seed-ROI correlation between each parcellation segment of the thalamus and its corresponding DMN ROIs were determined and compared with correlations with the remaining five non-corresponding ROIs. The hippocampus, precuneus, and sFG segments of the thalamus had significant RSFC seed-ROI correlations with their corresponding ROIs ($30.65 >$ average normalized z-scores > 3.20, P's < 0.05, Fig. 7 left). The precuneus segment of the thalamus further exhibited the strongest RSFC correlation to the precuneus ROI when compared with the other 5 ROIs (student's *t*-test [two-tailed, unequal variance], $P < 0.0001$).

No significant effect of gender (one-way MANOVA; dependent variables: resting-state seed-ROI correlations between thalamus segments [mPFC, hippocampus, sFG, and precuneus] and corresponding ROIs [mPFC, hippocampus, sFG, and precuneus]; fixed factor: gender) and no significant correlations were found between age and RSFC between the thalamus segments and corresponding ROIs (P's > 0.20).

Across thalamus segments, the strongest RSFC correlations to their non-corresponding segments were with the hippocampus and precuneus ROIs (hippocampus: $6.29 >$ average normalized z-scores > 4.256, P's < 0.0001; precuneus: $4.84 >$ average normalized z-scores > 2.039, P's < 0.05), while the AG consistently exhibited the lowest RSFC connectivity to all segments of the thalamus ($1.32 >$ average normalized z-scores > 0.03, P's > 0.10, Fig. 7 right). The RSFC in the mPFC ROI was also consistently negatively correlated with resting-state activity across the thalamus segments.

Comparing structure and function between the precuneus, thalamus, and DMN

In order to directly evaluate the relationship between structure and function within the DMN (including the precuneus) and with the thalamus, we correlated the mean FA value between a segment and ROI with the RSFC seed-ROI correlation between those same two regions. Since it is possible that the extent of connections was influenced by the use of distance correction during tractography (where streamlines between proximate ROIs were down-weighted compared with streamlines between ROIs farther apart from one another; the opposite effect would have occurred without the use of distance correction), we chose to use a structural metric that was not affected by our tractography methodology. While both FA and the extent of connections may be influenced by a crossing-fiber effect (further described in the *Discussion*), FA represents the least-processed metric. Mean FA and RSFC seed-ROI correlation values were thus evaluated across subjects for each segment—corresponding ROI pair. Across all three precuneus segments and all four thalamic segments, no significant correlations were found between mean FA value and RSFC seed-ROI correlation (P's > 0.10).

DISCUSSION

Here, we show strong structural and functional connectivity between the precuneus and the thalamus, as well as a structural representation of the DMN in both these regions. This is consistent with white matter pathways between the precuneus and thalamus and key regions of the DMN mediating their functional interactions. However, while the patterns between structural and functional connections were similar for some DMN ROIs, this was not the case for others. Most notably, we show that whereas the precuneus was most strongly structurally connected to the thalamus and minimally connected with the AG, the strongest functional connectivity of the precuneus was with the AG, mPFC and hippocampus. This differs from our findings of connectivity between the thalamus and AG, which showed consistently weak structural and functional connectivity, corroborating prior results by others

[Greicius et al., 2009]. These patterns of connectivity are summarized in Fig. 8 and described in more detail below.

Functional vs. Structural Connectivity

Previous studies have established a functional interaction between the precuneus and thalamus during changes in consciousness [Arthuis et al., 2009; Crone et al., 2015; Hannawi et al., 2015; He et al., 2014; Vanhaudenhuyse et al., 2010; Xie et al., 2011; Zhang and Li, 2012]. Here, we identified a map of structural and functional connectivity between these two regions. While both the precuneus and thalamus were found to be highly structurally connected to each other as well as to the hippocampus, mPFC, and sFG (in the case of the thalamus), our work found that strong structural connectivity did not always translate into strong functional connectivity between two regions. Indeed, while structural connectivity of the precuneus with the thalamus was the strongest when compared to connectivity with the DMN ROIs (where connectivity to the thalamus accounted for 68.11% of the precuneus volume as compared with the mPFC, which was the second strongest but accounted for only 18.94%), functional connectivity to the precuneus was stronger with the DMN ROIs (AG, mPFC, and hippocampus) than with the thalamus. This apparent discrepancy might reflect the fact that the thalamus and precuneus are highly connected regions that serve as hubs to which the signals from multiple resting-state networks converge [Bell and Shine, 2015]. As a result, despite the strong structural connectivity between them, they might appear to have less functional connectivity because of the mixing of incoming signals from the various networks with which they interact [Jbabdi et al., 2015; Schaefer et al., 2014].

Nevertheless, there was an overall significant correspondence between functional and structural connectivity pathways connecting the precuneus and thalamus. Significant RSFC seed-ROI correlations were found along pathways between some segments of the precuneus and thalamus and their corresponding ROIs. This may hint at a degree of resting-state specificity, where a DMN ROI often has the strongest RSFC seed-ROI correlation with areas in the precuneus and thalamus that receive the most structural connections from that ROI. However, specifically correlating the mean FA value between a precuneus or thalamus segment and its corresponding ROI with the strength of RSFC between the same two regions found no significant relationships. This is clearly illustrated in in the case of the AG, which maintains highly significant functional but low structural connectivity with the precuneus. As discussed above, these results may reflect signal interference among incoming signals from various functional networks with which they are connected.

Our finding that functional connectivity from the precuneus and thalamus to the DMN does not always follow structural connectivity as delineated by DTI differs from prior results reporting a significant relationship between RSFC and DTI connectivity between regions within the DMN [Greicius et al., 2009]. This prompts the notion that functional connectivity from the precuneus and thalamus to the rest of the DMN may occur via indirect axonal pathways or along smaller interneuron contacts [Cavanna and Trimble, 2006]. Functional connectivity may also be predominantly mediated though cortico-cortical connections, many of which are located in superficial white matter tracts that cannot be measured by tractography [Reveley et al., 2015]. In this respect, it was interesting that the AG had very low structural and functional connectivity with the thalamus, which was distinct from the other DMN regions. Finally, differences between structural and functional connectivity among the thalamus, precuneus, and DMN ROIs may reflect dynamic shifts in functional connectivity for hub regions in the brain [Thompson and Fransson, 2015; Yang et al., 2014].

We further found a strong negative correlation between the extent of probabilistic white matter connections and mean FA values, a phenomenon that was observed between the precuneus and thalamus, where increasing age from 23 to 35 years old was correlated with an increase in FA but decrease in the extent of connections between the two regions. This finding may be interpreted in two ways: (1) as evidence of white matter maturation within our young adult population as age advances [Barnea-Goraly et al. 2005], or (2) that smaller, denser connections may exist in regions with fewer major white matter pathways that help modulate functional connectivity between the thalamus, precuneus, and DMN and which cannot be resolved with current MRI strategies (see *Methodological Considerations* for further discussion).

Thalamus–Precuneus Connectivity

Impairment of consciousness has often been associated with deficits in the precuneus and thalamus [Crone et al., 2013]. We found a strong structural relationship between these two regions that could act as a pathway for modulation between the two during impaired consciousness. The precuneus primarily connects to regions of the thalamus that project to the parietal and occipital lobes—the same region occupied by the precuneus. This further suggests that connectivity between the precuneus and thalamus follows known thalamocortical pathways [as described in the Oxford Thalamic Connectivity Probability Atlas: Behrens et al., 2003]. These structural pathways are complemented by a significant RSFC seed-ROI correlation between the precuneus segment of the thalamus and precuneus, as well as between the thalamus segment of the precuneus and thalamus, confirming that the regions are in fact functionally connected.

We also found significant structural connectivity of both the precuneus and thalamus to the mPFC. Disruptions in connectivity of these areas have been hypothesized to

contribute to reduced consciousness [Crone et al., 2013]. Changes in structural connectivity in the DMN and along pathways connecting the precuneus and thalamus have further been correlated with behavioral signs of awareness in patients with disorders of consciousness [Fernandez-Espejo et al., 2012].

Thalamic connectivity to the DMN

The DTI findings on thalamic connectivity with the DMN are consistent with the thalamic origin and cortical endpoints of previously reported white matter thalamocortical tracts [Behrens et al., 2003]. The DTI analyses showed that the thalamus was most strongly connected to the precuneus, hippocampus, mPFC, and sFG. The largest hippocampus segment fell within the dorsal medial thalamic nucleus—a region associated with consciousness. The mesocircuit model [Giacino et al., 2014; Schiff, 2010] proposes that projections from the "arousal" system (i.e., basal forebrain and brainstem) and frontal network converging on the central thalamus help regulate consciousness [Schiff, 2008].

The DMN is associated with several functions including mind wandering and thinking [Christoff et al., 2009; Esposito et al., 2006]. The regions that are part of the DMN are inconsistently reported across studies, which has led to the suggestion of subsystems within the DMN. Among the regions that are not typically associated with the DMN but are occasionally included as a DMN region is the thalamus. Since prior studies [Hutchinson et al., 1999; Singh and Fawcett, 2008] have shown that regions of the DMN are deactivated with task performance (a finding that could be interpreted to reflect that they are deactivated since they are not critical for the task), this suggests that a DMN subsystem that includes the thalamus under conditions of decreased alertness or arousal may also play an important role in switching between internal and external awareness. The strong structural connections identified between the thalamus and regions key to consciousness [e.g., precuneus, hippocampus, and mPFC which is important in self-referential thought—Kurczek et al., 2015] support the notion described in a previous study [Fernandez-Espejo et al., 2012] that the thalamus plays a role in modulating the DMN during impaired consciousness.

Connectivity findings with the Angular Gyrus

The AG is a brain region that is fundamental for semantic processing [Seghier et al., 2010]. However, recent neuroimaging studies suggest that the AG serves a more general function besides its semantic processing role. Specifically, it has been proposed that the AG serves as a buffer of incoming internal or external information [Humphreys and Lambon Ralph, 2014]. As such, the AG is considered to be among the highest functionally connected areas in the brain [Buckner et al., 2009]. Consistent with this, we showed that the AG has among the strongest functional connectivity of the DMN ROIs with the precuneus. In contrast, a structural analysis revealed weak structural connectivity of the AG with the precuneus and thalamus. This suggests that connectivity of the AG might be mediated indirectly though cortico-cortical connections rather than predominantly relying on connections through white matter fibers, which are the ones being measured by DTI.

Methodological Considerations

Low structural connectivity between nearby regions could reflect the distance correction implemented during tractography, where streamlines between the precuneus and AG were down-weighted compared with those between other thalamic and DMN ROIs. However, the posterior (temporal and parietal) partitions of the thalamus demonstrated strong connectivity with the very proximal ventral precuneus, suggesting that distance correction may not be driving the lack of connectivity between the precuneus and the AG. In addition, results obtained from tractography without distance correction (see *Supporting Information*) similarly illustrate low structural connectivity between the precuneus and AG. Results concerning low structural connectivity to the AG may also reflect an inability to completely resolve crossing fibers that connect the AG to the precuneus and thalamus using a tractography analysis [Greicius et al., 2009; Mori and Zhang, 2006; Peled et al., 2006]. Alternatively it could reflect the possibility that fibers connecting the precuneus and AG might be located in superficial white matter tracts and hence are not accessible for detections with current DTI methods [Reveley et al., 2015]. This leaves the question of whether the above described AG findings are a consequence of our tractography methodology, or are an indication that connectivity of the AG to the precuneus and thalamus occurs via indirect connections or via cortico-cortical connections that are not detected by DTI and probabilistic tractography. It is also possible that recently identified differences in connectivity between the anterior versus posterior subdivision of the AG and DMN explain our low structural connectivity results: Uddin et al., 2010 found that the AG's anterior subdivision had significantly lower structural connectivity to regions in the DMN than the posterior segment. Not distinguishing between the two subdivisions could thus result in a misrepresentation of structural connectivity between the AG and other target ROIs.

In a similar manner, the finding of a negative correlation between mean FA and the extent of connections between the precuneus and thalamus coincides with the theory that mean FA decreases with an increasing number of connections due to a cross-fiber effect that cannot be resolved with standard tensor algorithms [Oouchi et al., 2007]. This crossing-fiber effect would mean that an observed decrease in mean FA does not indicate a decrease in fiber integrity,

but is instead a result of an increase in white matter connections that cannot be correctly resolved. Accordingly, the increase in mean FA (and decrease in extent of connections) observed with increasing age may be a product of the reduction in the number of fibers and the limitations of our tractography methodology. This possible limitation also applies to the finding of a significant negative correlation between the extent of connections and mean FA value between the thalamus and combined DMN ROIs.

CONCLUSION

Structural connectivity between the precuneus, thalamus, and DMN in healthy subjects provides a baseline for studying the effect of disorders that affect consciousness or interfere with self-awareness (such as addiction). In cases of impaired consciousness (including minimally conscious, vegetative, and coma states), future work should determine if functional changes among the DMN, precuneus, and thalamus are related to changes within these structural connections. Further work is also needed to understand the relationship between structural and functional connectivity for hubs that are dynamically changing as a function of brain activity, including consciousness.

REFERENCES

Andersson JLR, Skare S, Ashburner J (2003): How to correct susceptibility distortions in spin-echo echo-planar images: Application to diffusion tensor imaging. NeuroImage 20:870–888.

Arbabshirani MR, Damaraju E, Phlypo R, Plis S, Allen E, Ma S, Mathalon D, Preda A, Vaidya JG, Adali T, Calhoun VD (2014): Impact of Autocorrelation on Functional Connectivity. Neuroimage 102(02): 294–308.

Arthuis M, Valton L, Régis J, Chauvel P, Wendling F, Naccache L, Bernard C, Bartolomei F (2009): Impaired consciousness during temporal lobe seizures is related to increased long-distance cortical-subcortical synchronization. Brain 132(Pt 8):2091–101.

Barnea-Goraly N, Menon V, Eckert M, Tamm L, Bammer R, Karchemskiy A, Dant CC, Reiss AL (2005): White matter development during childhood and adolescence: A cross-sectional diffusion tensor imaging study. Cereb Cortex 5:1848–1854.

Behrens TE, Johansen-Berg H, Woolrich MW, Smith SM, Wheeler-Kingshott CA, Boulby PA, Barker GJ, Sillery EL, Sheehan K, Ciccarelli O, Thompson AJ, Brady JM, Matthews PM (2003): Non-invasive mapping of connections between human thalamus and cortex using diffusion imaging. Nat Neurosci 6: 750–757.

Bell PT, Shine JM (2015): estimating large-scale network convergence in the human functional connectome. Brain Connect 5: 565–574.

Buckner RL, Sepulcre J, Talukdar T, Krienen FM, Liu H, Hedden T, Andrews-Hanna JR, Sperling RA, Johnson KA (2009): Cortical hubs revealed by intrinsic functional connectivity: Mapping, assessment of stability, and relation to Alzheimer's disease. J Neurosci 29:1860–1873.

Cavanna AE, Trimble MR (2006): The precuneus: A review of its functional anatomy and behavioural correlates. Brain 129(Pt 3): 564–583.

Cauda F, Micon BM, Sacco K, Duca S, D'Agata F, Geminiani G, Canavero S. (2009): Disrupted intrinsic functional connectivity in the vegetative state. J Neurol Neurosurg Psychiatry 80: 429–431.

Christoff K, Gordon AM, Smallwood J, Smith R, Schooler JW (2009): Experience sampling during fMRI reveals default network and executive system contributions to mind wandering. Proc Natl Acad Sci U S A 106:8719–8724.

Crone JS, Soddu A, Höller Y, Vanhaudenhuyse A, Schurz M, Bergmann J, Schmid E, Trinka E, Laureys S, Kronbichler M (2013): Altered network properties of the fronto-parietal network and the thalamus in impaired consciousness. NeuroImage Clin 4:240–248.

Crone JS, Schurz M, Höller Y, Bergmann J, Monti M, Schmid E, Trinka E, Kronbichler M (2015): Impaired consciousness is linked to changes in effective connectivity of the posterior cingulate cortex within the default mode network. NeuroImage 110:101–109.

Della-Maggiore V, Chau W, Peres-Neto PR, McIntosh AR (2002): An empirical comparison of SPM preprocessing parameters to the analysis of fMRI data. NeuroImage 17:19–28.

Desikan RS, Ségonne F, Fischl B, Quinn BT, Dickerson BC, Blacker D, Buckner RL, Dale AM, Maguire RP, Hyman BT, Albert MS, Killiany RJ (2006): An automated labeling system for subdividing the human cerebral cortex on MRI scans into gyral based regions of interest. Neuroimage 31:968–980.

Esposito F, Bertolino A, Scarabino T, Latorre V, Blasi G, Popolizio T, Tedeschi G, Cirillo S, Goebel R, Di Salle F (2006): Independent component model of the default-mode brain function: Assessing the impact of active thinking. Brain Res Bull 70: 263–269.

Fernández-Espejo D, Soddu A, Cruse D, Palacios EM, Junque C, Vanhaudenhuyse A, Rivas E, Newcombe V, Menon DK, Pickard JD, Laureys S, Owen AM (2012): A role for the default mode network in the bases of disorders of consciousness. Ann Neurol 72:335–333

Fridman EA, Beattie BJ, Broft A, Laureys S, Schiff ND (2014): Regional cerebral metabolic patterns demonstrate the role of anterior forebrain mesocircuit dysfunction in the severely injured brain. Proc Natl Acad Sci U S A 111:6473–6478.

García-Panach J, Lull N, Lull JJ, Ferri J, Martínez C, Sopena P, Robles M, Chirivella J, Noé E (2011): A voxel-based analysis of FDG-PET in traumatic brain injury: Regional metabolism and relationship between the thalamus and cortical areas. J Neurotrauma 28:1707–1717.

Giacino JT, Fins JJ, Laureys S, Schiff ND (2014): Disorders of consciousness after acquired brain injury: The state of the science. Nat Rev Neurol 10:99–114.

Glasser MF, Sotiropoulos SN, Wilson JA, Coalson TS, Fischl B, Andersson JL, Xu J, Jbabdi S, Webster M, Polimeni JR, Van Essen DC, Jenkinson M (2013): The minimal preprocessing pipelines for the Human Connectome Project. NeuroImage 80: 105–124.

Greicius MD, Supekar K, Menon V, Dougherty RF (2009): Resting-state functional connectivity reflects structural connectivity in the default mode network. Cereb Cortex 19:72–78.

Gusnard DA, Raichle ME (2001): Searching for a baseline: Functional imaging and the resting human brain. Nat Rev Neurosci 2:685–694.

Hannawi Y, Lindquist MA, Caffo BS, Sair HI, Stevens RD (2015): Resting brain activity in disorders of consciousness: A systematic review and meta-analysis. Neurology 84:1272–1280.

He JH, Cui Y, Song M, Yang Y, Dang YY, Jiang TZ, Xu RX (2014): Decreased functional connectivity between the mediodorsal thalamus and default mode network in patients with disorders of consciousness. Acta Neurol Scand 131:145–151.

Humphreys GF, Lambon Ralph MA (2014): Fusion and fission of cognitive functions in the human parietal cortex. Cereb Cortex 25:3547–3560.

Hutchinson M, Schiffer W, Joseffer S, Liu A, Schlosser R, Dikshit S, Goldberg E, Brodie JD (1999): Task-specific deactivation patterns in functional magnetic resonance imaging. Magn Reson Imaging 17:1427–1436.

Jang JH, Jung WH, Kang DH, Byun MS, Kwon SJ, Choi CH, Kwon JS (2010): Increased default mode network connectivity associated with meditation. Neurosci Lett 487:358–362.

Jbabdi S, Sotiropoulos SN, Haber SN, Van Essen DC, Behrens TE (2015): Measuring macroscopic brain connections in vivo. Nat Neurosci 18:1546–1555.

Jenkinson M, Bannister P, Brady M, Smith S (2002): Improved optimisation for the robust and accurate linear registration and motion correction of brain images. NeuroImage 17:825–841.

Jones EG (1985): The Thalamus. New York: Plenum Press.

Jones EG, Powell TP (1970): Connexions of the somatic sensory cortex of the rhesus monkey. Brain 93:37–56.

Jones EG, Wise SP, Coulter JD (1979): Differential thalamic relationships of sensory-motor and parietal cortical fields in monkeys. J Comp Neurol 183:833–881.

Kurczek J, Wechsler E, Ahuja S, Jensen U, Cohen NJ, Tranel D, Duff M (2015): Differential contributions of hippocampus and medial prefrontal cortex to self-projection and self-referential processing. Neuropsychologia 73:116–126.

Laureys S, Goldman S, Phillips C, Van Bogaert P, Aerts J, Luxen A, Franck G, Maquet P (1999): Impaired effective cortical connectivity in vegetative state: Preliminary investigation using PET. Neuroimage 9:377–382.

Mori S, Zhang J (2006): Principles of diffusion tensor imaging and its applications to basic neuroscience research. Neuron 51: 527–539.

O'Muircheartaigh J, Keller SS, Barker GJ, Richardson MP (2015): White matter connectivity of the thalamus delineates the functional architecture of competing thalamocortical systems. Cereb Cortex 25:4477–4489.

Oouchi H, Yamada K, Sakai K, Kizu O, Kubota T, Ito H, Nishimura T. (2007): Diffusion anisotropy measurement of brain white matter is affected by voxel size: underestimation occurs in areas with crossing fibers. AJNR Am J Neuroradiol 28:1102–1106.

Peled S, Friman O, Jolesz F, Westin CF (2006): Geometrically constrained two-tensor model for crossing tracts in DWI. Magn Reson Imaging 24:1263–1270.

Reveley C, Seth AK, Pierpaoli C, Silva AC, Yu D, Saunders RC, Leopold DA, Ye FQ (2015): Superficial white matter fiber systems impede detection of long-range cortical connections in diffusion MR tractography. Proc Natl Acad Sci 112: E2820–E2828.

Sambataro F, Murty VP, Callicott JH, Tan HY, Das S, Weinberger DR, Mattay VS (2010): Age-related alterations in default mode network: Impact on working memory performance. Neurobiol Aging 31:839–852.

Schaefer A, Margulies DS, Lohmann G, Gorgolewski KJ, Smallwood J, Kiebel SJ, Villringer A (2014): Dynamic network participation of functional connectivity hubs assessed by resting-state fMRI. Front Hum Neurosci 8:195.

Schiff ND (2008): Central thalamic contributions to arousal regulation and neurological disorders of consciousness. Ann NY Acad Sci 1129:105–118.

Schiff ND (2010): Recovery of consciousness after brain injury: A mesocircuit hypothesis. Trends Neurosci 33:1–9.

Seghier ML, Fagan E, Price CJ (2010): Functional subdivisions in the left angular gyrus where the semantic system meets and diverges from the default network. J Neurosci 30:16809–16817.

Shirer WR, Ryali S, Rykhlevskaia E, Menon V, Greicius MD (2012): Decoding subject-driven cognitive states with whole-brain connectivity patterns. Cereb Cortex 22:158–165.

Singh KD, Fawcett IP (2008): Transient and linearly graded deactivation of the human default-mode network by a visual detection task. Neuroimage 41:100–112.

Skudlarski P, Constable RT, Gore JC (1999): ROC analysis of statistical methods used in functional MRI: Individual subjects. Neuroimage 9:311–329.

Soddu A, Vanhaudenhuyse A, Bahri MA, Bruno MA, Boly M, Demertzi A, Tshibanda JF, Phillips C, Stanziano M, Ovadia-Caro S, Nir Y, Maquet P, Papa M, Malach R, Laureys S, Noirhomme Q (2012): Identifying the default-mode component in spatial IC analyses of patients with disorders of consciousness. Hum Brain Mapp 33 :778–796.

Tanaka D Jr (1976): Thalamic projections of the dorsomedial prefrontal cortex in the rhesus monkey (Macaca mulatta). Brain Res 110:21–38.

Taylor VA, Daneault V, Grant J, Scavone G, Breton E, Roffe-Vidal S, Courtemanche J, Lavarenne AS, Marrelec G, Benali H, Beauregard M (2013): Impact of meditation training on the default mode network during a restful state. Soc Cogn Affect Neurosci 8:4–14.

Thompson WH, Fransson P (2015): The frequency dimension of fMRI dynamic connectivity: Network connectivity, functional hubs and integration in the resting brain. Neuroimage 121:227–242.

Tobias TJ (1975): Afferents to prefrontal cortex from the thalamic mediodorsal nucleus in the rhesus monkey. Brain Res 83: 191–212.

Tomasi D, Volkow ND (2010): Functional connectivity density mapping. Proc Natl Acad Sci U S A 107:9885–9890.

Tomasi D, Volkow ND (2011): Association between functional connectivity hubs and brain networks. Cereb Cortex 21: 2003–2013.

Tomasi D, Volkow ND (2012): Gender Differences in Brain Functional Connectivity Density. Hum Brain Mapp 33: 849–860.

Uddin LQ, Supekar K, Amin H, Rykhlevskaia E, Nguyen DA, Greicius MD, Menon V (2010): Dissociable connectivity within human angular gyrus and intraparietal sulcus: Evidence from functional and structural connectivity. Cereb Cortex 20:2636–2646.

Uğurbil K, Xu J, Auerbach EJ, Moeller S, Vu AT, Duarte-Carvajalino JM, Lenglet C, Wu X, Schmitter S, Van de Moortele PF, Strupp J, Sapiro G, De Martino F, Wang D, Harel N, Garwood M, Chen L, Feinberg DA, Smith SM, Miller KL, Sotiropoulos SN, Jbabdi S, Andersson JL, Behrens TE, Glasser MF, Van Essen DC, Yacoub E (2013): Pushing spatial and temporal resolution for functional and diffusion MRI in the Human Connectome Project. Neuroimage 80:80–104.

Utevsky AV, Smith DV, Huettel SA (2014): Precuneus is a functional core of the default-mode network. J Neurosci 34: 932–940.

Van Essen DC, Smith SM, Barch DM, Behrens TE, Yacoub E, Ugurbil K (2013): The WU-Minn Human Connectome Project: An overview. Neuroimage 2013 80:62–79.

Vanhaudenhuyse A, Noirhomme Q, Tshibanda LJ, Bruno MA, Boveroux P, Schnakers C, Soddu A, Perlbarg V, Ledoux D, Brichant JF, Moonen G, Maquet P, Greicius MD, Laureys S, Boly M (2010): Default network connectivity reflects the level of consciousness in non-communicative brain-damaged patients. Brain 133(Pt 1):161–171.

White NS, Alkire MT (2003): Impaired thalamocortical connectivity in humans during general-anesthetic-induced unconsciousness. Neuroimage 19(2 Pt 1):402–411.

Woolrich MW, Ripley BD, Brady M, Smith SM (2001): Temporal autocorrelation in univariate linear modelling of FMRI data. NeuroImage 14:1370–1386.

Xie G, Deschamps A, Backman SB, Fiset P, Chartrand D, Dagher A, Plourde G (2011): Critical involvement of the thalamus and precuneus during restoration of consciousness with physostigmine in humans during propofol anaesthesia: A positron emission tomography study. Br J Anaesth 106:548–557.

Yang Z, Chang C, Xu T, Jiang L, Handwerker DA, Castellanos FX, Milham MP, Bandettini PA, Zuo XN (2014): Connectivity trajectory across lifespan differentiates the precuneus from the default network. Neuroimage 89:45–56.

Zhang S, Li CS (2012): Functional connectivity mapping of the human precuneus by resting state fMRI. Neuroimage 59: 3548–3562.

Zhang D, Snyder AZ, Shimony JS, Fox MD, Raichle ME (2010): Noninvasive functional and structural connectivity mapping of the human thalamocortical system. Cereb Cortex 20: 1187–1194